Special Section:
Soil Architecture and Function

Charmaine Q. Qiu
Jie Han
Hui Gao
Lian-Ping Wang*
Yan Jin*

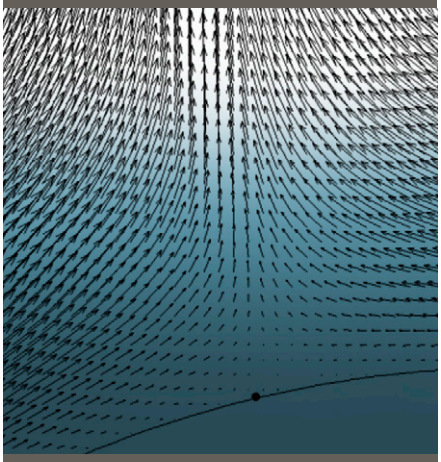

Pore-scale model simulations of colloid trajectories were used to systematically study the retention of colloids at the secondary energy minimum. The main conclusion is that the colloid retention rate depends nonlinearly on the solution ionic strength and flow speed, consistent with mechanistic explanations and experimental observations.

C.Q. Qiu, H. Gao, and L.-P. Wang, Dep. of Mechanical Engineering, Univ. of Delaware, Newark, DE 19716; and J. Han and Y. Jin, Dep. of Plant and Soil Sciences, Univ. of Delaware, Newark, DE 19716-3140. *Corresponding authors (lwang@udel.edu; yjin@udel.edu).

Vadose Zone J.
doi:10.2136/vzj2011.0071
Received 27 June 2011.

Pore-Scale Numerical and Experimental Investigation of Colloid Retention at the Secondary Energy Minimum

Mechanistic understanding of colloid retention and transport in porous media is important in many environmental processes and applications. In this study, we characterized and quantified colloid retention under unfavorable attachment conditions through modeling coupled with pore-scale experiments, focusing on the effects of solution ionic strength and interstitial flow speed. A computational approach was developed to simulate the motion of colloids suspended in pore-scale flow through a network of grain packing in a bounded channel. Simulation results showed that colloids could only be retained at the secondary energy minimum (SEmin) due to the presence of the high repulsive energy barrier (above 1500 kT). The fraction of colloids that can move into the SEmin well and be subsequently retained by the attractive van der Waals force is controlled by the competition of hydrodynamic transport along the streamline and Brownian shifting across the streamline. The tangential hydrodynamic force could slowly drive retained colloids toward the rear stagnation region along the surface, leading to accumulation of retained colloids. The retention at SEmin is dynamically irreversible when the SEmin depth reaches about −4 kT. These mechanistic insights explain well the dependence of the retention ratio on flow speed at a given ionic strength as well as the saturation of the retention ratio with ionic strength at a prescribed flow speed. Furthermore, for a given ionic strength, there is a critical flow speed below which Brownian motion dominates the colloid retention rate, leading to a very strong dependence of surface coverage on flow speed. These simulation results were confirmed by experimental confocal-microscopy observations in capillary porous channels as well as by other published results, supporting the mechanistic findings.

Abbreviations: DLVO, Derjaguin–Landau–Verwey–Overbeek; SEmin, secondary energy minimum.

Knowledge of the fate and transport of colloidal-sized particles in porous media is important in many processes and applications. These include better design of sand and membrane filtration systems for water and wastewater treatment, improving the efficiency of bioremediation and bioaugmentation, and more accurate prediction of the transport potential of colloid-bound contaminants, pathogens, and nanoparticles (McCarthy and Zachara, 1989; Saiers and Hornberger, 1996; Kretzschmar et al., 1999; Saiers, 2002; Zhuang et al., 2003, 2005; Grolimund and Borkovec, 2005; Chen et al., 2005). The concerns about contamination of groundwater with pathogens (e.g., viruses, bacteria, and protozoa, also referred to as biocolloids) and colloid-facilitated transport of radionuclides, metals, and strongly sorbing organics have led to intensive research in recent years on colloid retention, release, and transport behavior in subsurface porous media.

Most previous studies on colloid retention and transport in porous media used the approach of conducting laboratory column experiments and numerical simulations of the resulting breakthrough curves (Elimelech and O'Melia, 1990a; Ryan and Elimelech, 1996; Saiers and Lenhart, 2003; Bradford et al., 2003, 2007; Shen et al., 2007), which presents normalized colloidal concentrations in effluent as a function of time or pore volumes. These macroscopic-scale experiments and corresponding model exercises have provided information on the extent of colloid retention as the colloids in suspension move through columns packed with sand, glass beads, or soil. This "black box" approach of monitoring colloid concentrations in effluent and analyzing breakthrough curves is not conducive, however, for elucidating the mechanisms that are responsible for colloid retention.

In recent years, there has been significant effort devoted to using microscopic techniques and micromodels of various designs (Wan and Wilson, 1994; Sirivithayapakorn

and Keller, 2003; Lazouskaya et al., 2006) for studying colloid transport and retention behavior at the pore scale (1 μm–1 mm). Direct visualization of colloid interfacial reactions using micromodels is a promising alternative complementing the traditional approaches and providing a unique opportunity for mechanistic investigations at the pore scale. This microscopic approach has been successfully used to help explain and clarify phenomena observed in macroscopic experiments and simulations. Colloid retention mechanisms, such as deposition at the solid–water interface; removal at grain–grain contacts; attachment at the air–water interface, air–water–solid interface, or the contact line; and film straining, have been identified through visualization and analysis of pore-scale images (Wan and Wilson, 1994; Wan and Tokunaga 1997; Sirivithayapakorn and Keller, 2003; Weisbrod et al., 2003; Crist et al., 2004, 2005; Zevi et al., 2005; Lazouskaya et al., 2006).

While pore-scale experiments have contributed significantly to the mechanistic investigation of colloid retention in porous media, parallel developments in conceptual models and related numerical methods are rather limited. In general, there are two components to pore-scale dynamic modeling: simulation of liquid flow and simulation of transport of colloids by liquid flow and interactions of colloids with grain surfaces. Simulation of colloid retention and transport could be performed in either an Eulerian or a Lagrangian fashion. The Eulerian approach considers the distribution of particle concentrations (a mean-field variable) across space and time (Bradford et al., 2003; Bradford and Toride, 2007) and yields an extended advection–dispersion equation with source–sink terms that parameterize the effects of colloid–surface interactions. The specification of these source–sink terms involves modeling assumptions (i.e., constant deposition and release rate coefficients) that may not be applicable to the so-called unfavorable conditions where colloids and collectors have the same charge, which are commonly encountered in natural porous media (Bradford and Toride, 2007). Moreover, due to the associated coarse-graining or averaging, the Eulerian approach cannot provide detailed description of pore-scale colloid retention and movement within the secondary energy minimum. The Lagrangian approach focuses on individual colloids and tracks their position with time according to Newton's second law. While the Lagrangian approach is computationally more expensive than the Eulerian approach, it provides a direct mechanistic description of transport that can be helpful for elucidating the relevant processes. Furthermore, the discrete nature of the Lagrangian approach makes it much more feasible to include complex interactions with the grain surface. For these reasons, most previous mechanistic studies adopted the Lagrangian trajectory approach.

Under the Lagrangian trajectory approach, unit-cell-based flow representation found widespread use in previous studies, including the sphere-in-cell model (Happel, 1958; Rajagopalan and Tien, 1976) and two-dimensional (Payatakes et al., 1974a,b) and three-dimensional (Paraskeva et al., 1991; Burganos et al., 1992, 1994) constriction tube models. These unit-cell models take advantage of the symmetrical properties of flow passage and make use of either the available analytical creeping-flow solution or numerical solution of viscous flow in simple model geometries, but they provide only a phenomenological representation of soil pore-scale geometry without consideration of grain–grain contact and grain surface irregularities. Cushing and Lawler (1998) considered grain–grain contact in a unit cell representing a densely packed regular array of spheres and solved the creeping fluid flow using Galerkin's method developed by Snyder and Stewart (1966). They then solved the trajectories of the colloids to study colloid attachment efficiency. Johnson et al. (2007) adopted the same unit-cell approach to solve pore-scale flow and a trajectory approach for colloids; they confirmed colloid retention in flow stagnation zones and wedging in grain-to-grain contacts. They also indicated the need to solve viscous flows through pore domains rendered from actual porous media in order for such an approach to become a useful quantitative tool.

To our knowledge, there have been very few attempts in the colloidal literature to simulate colloid transport and retention in complex pore-scale flows beyond unit cells. Berry et al. (2004) used a mesoscopic approach known as *smoothed particle hydrodynamics* to study contaminant transport and deposition in a complex two-dimensional porous flow. Very recently, the lattice-Boltzmann approach has been applied to simulate pore-scale flow in realistic three-dimensional porous media to help quantify the transport and retention of colloids and contaminants in complex systems (e.g., Li et al., 2010; Long and Hilpert, 2008, 2009; Long et al., 2010).

In the subsurface environment, where colloids and grain sediments typically carry a negative surface charge under the prevailing pH conditions, colloid retention occurs mainly in the secondary energy minimum (SEmin) due to the presence of repulsive energy. The SEmin well is located at a finite distance from the collector surface, resulting from the attractive van der Waals interaction. Retention at the SEmin differs from deposition at the primary energy minimum in several ways. First, if the SEmin well is not very deep, retention at the SEmin can be *dynamically* reversible due to Brownian motion or unsteady hydrodynamics. Second, the retention at SEmin is *chemically* reversible when the solution chemical conditions are altered, as shown experimentally by Hahn et al. (2004) and Shen et al. (2007), who found that retained colloids could be released back to the flow once the SEmin was removed, for example, by flushing the column with deionized water. Third, retained colloids at the SEmin could drift tangentially along the collector surface (Johnson et al., 2007; Li et al., 2010), leading to often nonuniform concentrations of retained colloids. Experimentally, Kuznar and Elimelech (2007) observed particle aggregation around rear stagnation points.

These unique and complex characteristics of colloid retention at the SEmin also motivated some recent computational studies. Hahn and O'Melia (2004) developed a Brownian dynamics–Monte Carlo model to simulate the movement of Brownian particles near

a rotating disk collector under unfavorable chemical conditions. They explicitly demonstrated colloid retention at the SEmin in their simulation. Johnson et al. (2007), using a three-dimensional unit-cell flow model, examined colloid retention under unfavorable conditions and demonstrated capture of the colloids by the SEmin. Reversibility of colloid retention in the SEmin was investigated by Li et al. (2010), who showed that this reversible capture could increase the colloid residence time in porous media. It is reasonable to expect that colloid retention increases as the depth of the SEmin increases (Johnson et al., 2007; Li et al., 2010); however, the transition process from reversible transport to nonreversible retention has not been fully studied.

Another general observation is that the colloid retention ratio (i.e., the ratio of the number of retained colloids to the total number of colloids injected) decreases as the flow speed increases (Unni and Yang, 2005; Yiantsios and Karabelas, 2003; Prieve and Lin, 1980; Shen et al., 2010). Most studies, however, are qualitative in nature. In this study, we developed a computational approach targeted for modeling colloid transport and retention in a pore network with arbitrary grain packing by combining a general pore-scale flow simulation using the lattice-Boltzmann approach with direct Lagrangian tracking of individual colloids. The main focus of our study was to examine the effects of solution ionic strength and interstitial flow speed on colloid retention at the SEmin in saturated porous media. In addition, visualization experiments were conducted via confocal microscopy and the results were compared with model simulations. The colloids considered in this study were sulfate-modified latex microspheres, which are amphiphilic in nature and may serve as a good model for biocolloids such as viruses.

The Computational Approach

Pore Geometry Model and Viscous Flow Simulation

In this study, we adopted a two-dimensional model approach (Gao et al., 2008). The grains were modeled as circular cylinders. The elemental flow domain consisted of seven grain cylinders (Fig. 1a), and periodic extension in the y direction was used to represent a porous channel of arbitrary length. This two-dimensional setting was used to mimic a plane slice of a three-dimensional channel of 0.8- by 0.8-mm cross-section, packed with spherical glass beads of 0.20-mm diameter, as used in our confocal visualization microchannel experiments (Fig. 1b). The channel width H was thus set to 0.8 mm and the periodic length L in the y direction was 0.282 mm, while the diameter of the cylinders was set to 0.154 mm. The channel depth in the direction normal to the plane shown in Fig. 1a was assumed to equal the cylinder radius (a_{cyl} = 0.077 mm) and one cell pore volume was defined as the volume of the pore space area shown in Fig. 1a times 0.077 mm. In view of the relatively slow retention rate at the grain scale and because such a long physical time interval is required for reliable statistics, a two-dimensional model is computationally more efficient than a three-dimensional model. A no-slip velocity condition was applied on the two sidewalls at $x = 0$ and $x = H$ and on the surfaces of the seven glass cylinders. The centers of the seven cylinders were located at (0.2, 0.0 mm), (0.4, 0.0 mm), (0.6, 0.0 mm), (0.1, 0.141 mm), (0.3, 0.141 mm), (0.5, 0.141 mm), and (0.7, 0.141 mm), respectively.

At an initial time $t = 0$, the fluid is at rest. Flow is then driven by a constant pressure gradient or a body force in the y direction. The body force per unit volume was set to $F_B = 8\rho\nu U_c/H^2$, where ν and ρ are the fluid kinematic viscosity and density, respectively, and U_c is the centerline velocity of the channel at long times when the body force is balanced by the viscous effects if there are no glass cylinders in the channel. The magnitude of U_c is adjusted to yield a Darcy or interstitial velocity relevant to the environmental conditions (1–8 m/d, similar to the values used in Tong and Johnson [2006] and Bradford et al. [2007]). A steady-state flow develops when the driving force is balanced by the sum of the viscous drags on the seven cylinders and the channel walls. This steady-state viscous flow is used to study the transport of colloids.

The methods to simulate slow viscous flow in the model geometry have been described in Gao et al. (2008) and the physical parameters were detailed in Gao et al. (2008, Table 1). Two computational

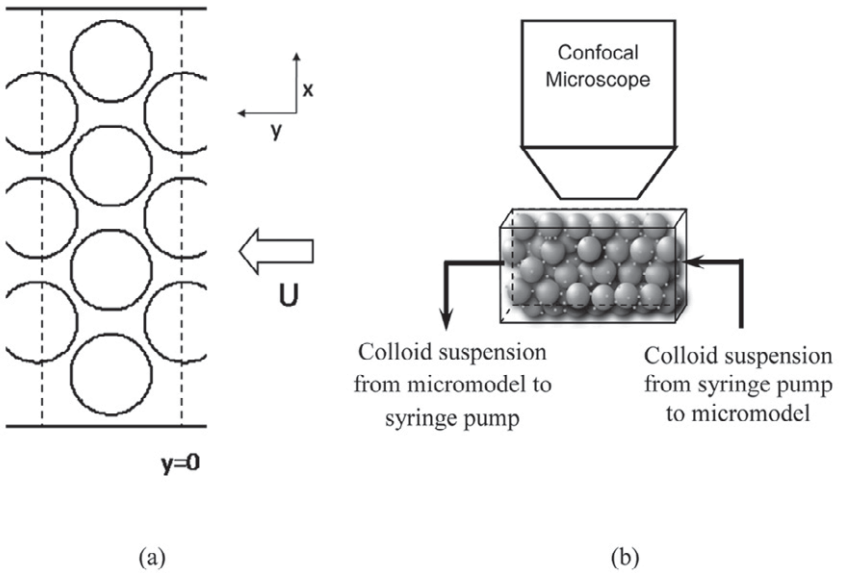

Fig. 1. (a) A two-dimensional geometric model, where the elemental flow domain marked by the two dashed lines consists of seven grain cylinders in a channel and the periodic extension of the domain provides a porous channel of any length in the y direction, with U as the interstitial mean flow velocity; (b) a schematic diagram of the experimental setup—the glass channel packed with glass beads was observed with a confocal microscope.

Table 1. Properties of colloids and glass beads at 20°C.

Property	Sulfate colloids	Glass beads
Diameter	1 μm	0.18– 0.25 mm
Zeta potential at ionic strength, mV		
0.001 mol/L	−85.13	−68.74†
0.01 mol/L	−87.97	−66.25†
0.03 mol/L	−75.00	−60.00
0.05 mol/L	−60.00	−55.00†
0.1 mol/L	−45.56	−41.31†
0.3 mol/L	−26.91	−18.00‡
Solid surface tension component, mJ/m^2		
Lifshitz–van der Waals component (γ_S^{LW})	43.59	41.70§
Electron-acceptor component (γ_S^+)	0	1.100§
Electron-donor component (γ_S^-)	5.584	44.50§
Solid total surface tension (γ_S) from Eq. [4]	43.59	55.69§

† From Johnson et al. (2007).
‡ From Elimelech and O'Melia (1990b).
§ From Chen and Flury (2005).

methods were simultaneously applied: a mesoscopic method known as the lattice-Boltzmann method and a macroscopic Navier–Stokes-based hybrid method (Physalis) developed by Zhang and Prosperetti (2003, 2005). The mesoscopic lattice-Boltzmann method (Chen and Doolen, 1998; Yu et al., 2003) is an unconventional approach based on a kinetic formulation and has several advantages over the traditional Navier–Stokes-based computational fluid dynamics, especially when irregular grains and random packing of grains are to be represented. Both methods are capable of accurately resolving the viscous flow field. Using two completely different methods enabled us to self-validate the computational approach because direct experimental measurement of pore-scale viscous flow is not feasible. Thorough descriptions of the two methods and their rigorous validation were presented in Gao et al. (2008), who showed that the two methods led to almost identical local flow fields.

The pore-scale flow is characterized by strong variations in the local flow speed and direction, as well as variations in the curvature of flow streamlines. Vector plots of flow velocity fields are displayed in Fig. 2. There is a front stagnation point and rear stagnation point on each grain collector. The transverse flow (x-component) velocity is comparable to the velocity in the y direction due to the distortion of the flow by the grain particles. The grain particles create a very strong resistance to the flow, as evidenced by the fact that the mean flow speed is only 0.26% of the centerline velocity U_c in an open or empty channel.

Simulation of Transport and Retention of Colloids

Once the pore-scale fluid flow reached steady state, colloids were injected uniformly from the inlet of the channel with a velocity equal to the local fluid velocity. The concentration of colloids was set to 5 mg/L. This corresponds to a concentration of 9050 colloids/mL of the liquid volume. If the two-dimensional geometric model is assumed to represent a slice of thickness equal to the glass bead radius, then the above concentration corresponds to 66.3 colloids in the periodic fluid domain shown in Fig. 1a. Because this concentration is very low, the fluid flow was assumed to be unaffected by the presence of the colloids. Each colloid was tracked using the following equations of motion in the normal and tangential directions:

$$m_c \frac{dV_{i,n}}{dt} = F_{i,n}^{drag} + F_{i,n}^{C} + F_{i,n}^{B} \quad [1]$$

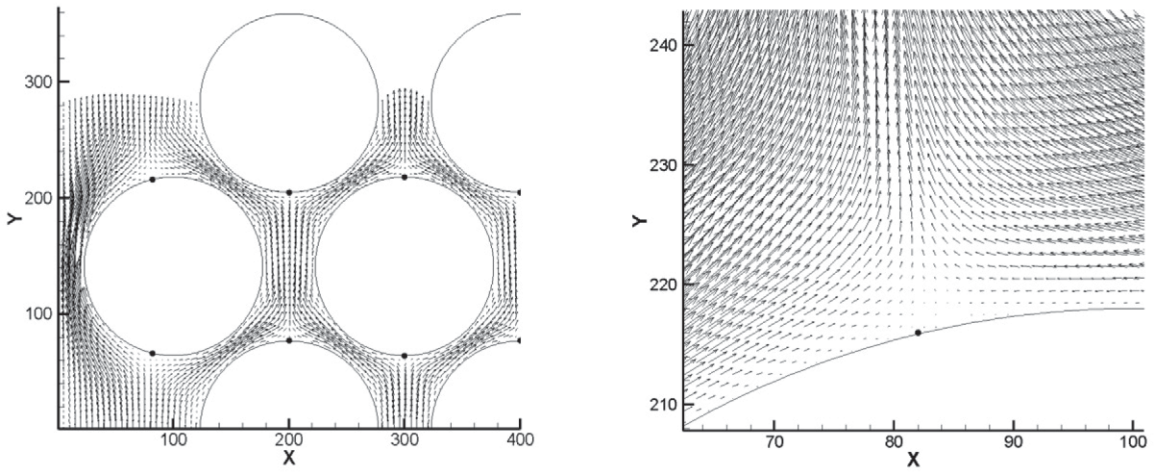

Fig. 2. Vector plots of the flow velocity field from the model simulation: (a) the left half of the first periodic domain (note that the symmetry and periodic nature of the flow can be used to generate flow in other regions); (b) a close-up view of the flow field around the rear stagnation point for the glass bead on the very left in (a). The unit for the coordinates is 1 μm.

$$m_c \frac{dV_{i,t}}{dt} = F_{i,t}^{drag} + F_{i,t}^{B} \quad [2]$$

where $V_{i,n}$ and $V_{i,t}$ (m/s) are the velocities of a colloid in the normal and tangential directions, respectively, m_c (kg) is the mass of the colloid, and t (s) is time. The forces acting on the colloid include the colloidal interaction force $F_{i,n}^{C}$, normal and tangential hydrodynamic drag components $F_{i,n}^{drag}$ and $F_{i,t}^{drag}$, and normal and tangential Brownian force components $F_{i,n}^{B}$ and $F_{i,t}^{B}$. Their formulations are described in the Appendix. The normal direction is defined as the direction perpendicular to the nearest solid surface (grain or channel wall), pointing into the fluid domain. Due to the similar magnitude of colloid density (1055 kg/m^3) and that of water (1000 kg/m^3), gravity and the buoyant force almost cancel each other out and thus were not considered.

Away from a collector surface, a colloid trajectory is only affected by the drag force and Brownian force and the time step can be made larger than the Stokes relaxation time of a colloid, τ_p, as long as the flow velocity changes slowly. The proper requirement for the time step size is $dt << D_g/U_0$, where D_g is the grain diameter and U_0 is the interstitial flow velocity. Close to a collector surface, however, the time step has to be made much smaller (by as much as two orders of magnitude in our simulations) so that the colloidal force will not change significantly during dt. We reduced the time step size when the colloid approached a collector and the Derjaguin–Landau–Verwey–Overbeek (DLVO) force became active (with a gap distance at 200 nm or less depending on the DLVO profile). More precisely, when a colloid entered the SEmin region, the time step was reduced such that any change in the DLVO energy during the colloid displacement within one time step was much smaller than the height of the repulsive energy barrier. For the physical conditions considered in this study, the energy barrier is high (typically >1500 kT) and colloids cannot cross the energy barrier to deposit at the primary energy minimum. Colloids could enter the SEmin, however, due to the attractive Lifshitz–van der Waals force and Brownian motion. This aspect is discussed in more detail below. It is very important to use a small enough time step to avoid any numerical artifact that causes colloids to cross the energy barrier.

Colloid transport in the model porous media was simulated for a range of interstitial flow velocities (2–150 m/d). In the simulations, we used the properties measured for sulfate-modified latex particles and glass beads (see below) as input parameters so that the modeling results could be directly compared with the experimental results. The colloid concentration was fixed at 5 mg/L in all simulations. Up to 6000 colloids were injected at the inlet depending on the flow speed. Note that the computation time is roughly inversely proportional to the flow speed.

We must note that a fine mesh is needed to accurately capture the trajectory of a colloid near a glass bead. As shown in Fig. 2, the flow velocity exhibits a high local gradient, particularly near the front and rear stagnation points. We found that an insufficient mesh resolution tended to overestimate the local fluid velocity at a colloid location near a collector surface, leading to a higher number of colloids retained at the SEmin. For example, we tested three flow-simulation mesh resolutions (regular mesh 400 by 141, fine mesh 800 by 282, and extremely fine mesh 1600 by 564) for the case of an ionic strength (IS) = 0.1 mol/L and a flow speed of 8 m/d and obtained 1444, 864, and 810 retained colloids, respectively, when 6000 colloids were injected. This demonstrates that the result appears to converge at the higher mesh resolutions. All the results shown below are based on the fine flow mesh of 800 by 282.

Micromodel Experiments Using Confocal Microscopy

Colloids and Glass Beads

Glass beads (Potters Industries, Chelmsford, MA) with diameters of 0.18 to 0.25 mm were used in the micromodel experiments. A procedure following Han et al. (2006) was used to remove impurities from the glass bead surfaces. The colloids used were sulfate-modified yellow-green latex microspheres (Invitrogen Corp., Carlsbad, CA) with a mean diameter of 1 μm and a density of 1.055 g/cm^3. These microspheres are stabilized by sulfate functional groups with a low pK_a (<2, where pK_a is the negative logarithm of the acid dissociation constant) and therefore are negatively charged at pH > 2. They are also hydrophobic and have a contact angle with water at ~80°C so are considered amphiphilic. Colloidal suspensions, according to the manufacturer, are stable up to 0.3 mol/L univalent electrolyte concentrations. Zeta potentials of the colloids were determined in pH 7.5 buffered solutions (NaCl and $NaHCO_3$) at ionic strengths of 0.001, 0.01, 0.1, and 0.3 mol/L by measuring their electrophoretic mobility using a zetasizer (Zetasizer nano series ZS, Malvern Instruments, Malvern, UK). Electrophoretic mobility was converted to ζ potential using the Smoluchowski equation (Overbeek, 1952). Calculated ζ potential values from the measured electrophoretic mobilities at different ionic strengths and pH 7.5 are summarized in Table 1.

Solid (glass or colloid) surface thermodynamic parameters (Lifshitz–van der Waals component, γ_S^{LW}; electron-acceptor component, γ_S^+; and electron-donor component, γ_S^-) used for the colloidal force calculations (Eq. [A9–A10], γ_2 for glass surface and γ_1 for colloid) can be determined using contact angle values of colloids and glass beads with one apolar liquid (diiodomethane) and two polar liquids (water and glycerol). We measured the contact angles of colloids in the three liquids following the procedure described below.

A droplet of colloid suspension obtained from the manufacturer (without further treatment) was put on a glass cover slip and dried at room temperature to form a uniform monolayer of colloidal film. Contact angle measurements were made using a light microscope

Table 2. Values of the surface tension components (total surface tension γ_L, Lifshitz–van der Waals component γ_L^{LW}, Lewis acid–base component γ_L^{AB}, electron-acceptor parameter γ_L^+, and electron-donor parameter γ_L^-) of test liquids used for contact angle measurements (Wu et al. 1995) and measured contact angle of sulfate-latex microspheres with each test liquid.

Liquid	γ_L	γ_L^{LW}	γ_L^{AB}	γ_L^+	γ_L^-	Contact angle
	mJ/m^2					°
Diiodomethane	50.8	50.8	0	~0	0	31.51
Glycerol	64	34	30	3.92	57.4	74.74
Water	72.8	21.8	51	25.5	25.5	79.94

connected with an AxioCam (Zeiss Axioskop 2 microscope, Carl Zeiss MicroImaging, Thornwood, NY). For each liquid (i.e., diiodomethane, water, or glycerol), a tiny droplet of that liquid was placed on the colloidal film with a syringe needle, and pictures were captured and analyzed. A total of three measurements were taken to obtain an averaged contact angle value for each liquid.

Surface thermodynamic properties of a solid and a liquid are related to each other by the liquid–solid contact angle θ according to the van Oss–Chaudhury–Good equation (van Oss, 1994):

$$(1+\cos\theta)\gamma_L = 2\left(\sqrt{\gamma_S^{LW}\gamma_L^{LW}} + \sqrt{\gamma_S^+\gamma_L^-} + \sqrt{\gamma_S^-\gamma_L^+}\right) \quad [3]$$

where γ is the component of surface tension (J/m^2) with subscript *S* denoting solid and *L* denoting liquid. The parameters γ, γ^{LW}, γ+, and γ^- are related through the following relationship:

$$\gamma = \gamma^{LW} + 2\sqrt{\gamma^-\gamma^+} \quad [4]$$

The components of surface tension for each liquid are known and listed in Table 2. Three equations with three unknowns (γ_S^+, γ_S^-, and γ_S^{LW}) were written by incorporating the surface tension components of each liquid and its corresponding contact angle and solved to obtain the surface thermodynamic properties of the colloids and glass beads. Sulfate-latex microspheres have contact angles of 31.51, 74.74, and 79.94° with diiodomethane, glycerol, and water, respectively (Table 2). Calculated surface tension components indicated a close relationship between colloidal surface hydrophobicity and the electron-donor component of the surface tension (γ_S^-), which is much greater than the electron-acceptor component (γ_S^+). A similar trend has also been observed in other studies (Chen and Flury, 2005; Wu, 2001).

Experimental Setup and Procedures

Components of the experimental setup included a glass capillary packed with glass beads (referred to as a micromodel), a syringe pump, and a confocal microscope (Fig. 1b). The capillary used in this study had a square cross-section of 0.8 by 0.8 mm and a porosity of 0.425. The inlet and outlet ends of the capillary were each covered with a nylon membrane with 20-μm pore openings (Spectra/Mesh, Spectrum Laboratories, Rancho Dominguez, CA) to keep the glass beads tightly packed in the capillary. A syringe pump (PHD 22/2000, Harvard Apparatus, Holliston, MA) was used to provide saturated and stable flow at a constant rate to the micromodel. A new micromodel was used for each experiment.

Experiments examining the retention and transport behavior of sulfate-latex microspheres in the packed capillaries under saturated flow were conducted and images were recorded with a laser scanning confocal microscope (Carl Zeiss Axiovert 200M equipped with LSM 510, Carl Zeiss, Stuttgart, Germany) at different solution ionic strengths (0.001 and 0.1 mol/L) and fluid velocities (5.3 and 53 m/d) with pH adjusted to 7.5. Ten milligrams per liter fluorescein with a fluorescence emission peak at 545 nm (Uthirakumar et al., 2005) was added to the buffer solution to provide the fluid with a yellow-green background that facilitated better viewing and acquisition of higher quality images. For each experiment, colloid-free buffer solution was first pumped through the micromodel (for at least 10 pore volumes) until chemical equilibrium and steady-state flow had been established; the input was then switched to the colloidal suspension containing 5 mg/L sulfate-latex microspheres.

Results and Discussion

Electrokinetic Potentials and Colloidal Interaction Energy

As shown in Table 1, the ζ potentials of both colloids and glass beads are negative across the range of solution ionic strength tested, indicating that the experimental conditions were unfavorable for colloid deposition at the primary energy minimum. For the colloids, a slight decrease in the ζ potential was observed as the ionic strength increased from 0.001 to 0.01 mol/L, while a much more significant increase occurred when the ionic strength increased from 0.01 to 0.3 mol/L. The minimum ζ potential observed at 0.01 mol/L is a common feature of sulfate-modified latex colloids, which was also reported elsewhere (Elimelech and O'Melia 1990b). As ionic strength increases, co-ions (Cl^- in this study) entering into the region adjacent to the colloidal surfaces due to hydrophobic interactions (sulfate microspheres have a contact angle of ~80° with water) reduce the electrokinetic potential of the particles and are responsible for the initial decrease in the ζ potential. At the same time, shrinking of the electrostatic double layer and neutralization of the surface charge as the ionic strength increases tends to increase the electrokinetic potential. These two processes reach equilibrium at 0.01 mol/L, above which compression of the electrostatic double layer and charge screening become the dominate mechanisms and therefore result in a constant increase in the ζ potential as the ionic strength continues to increase (Elimelech and O'Melia, 1990c).

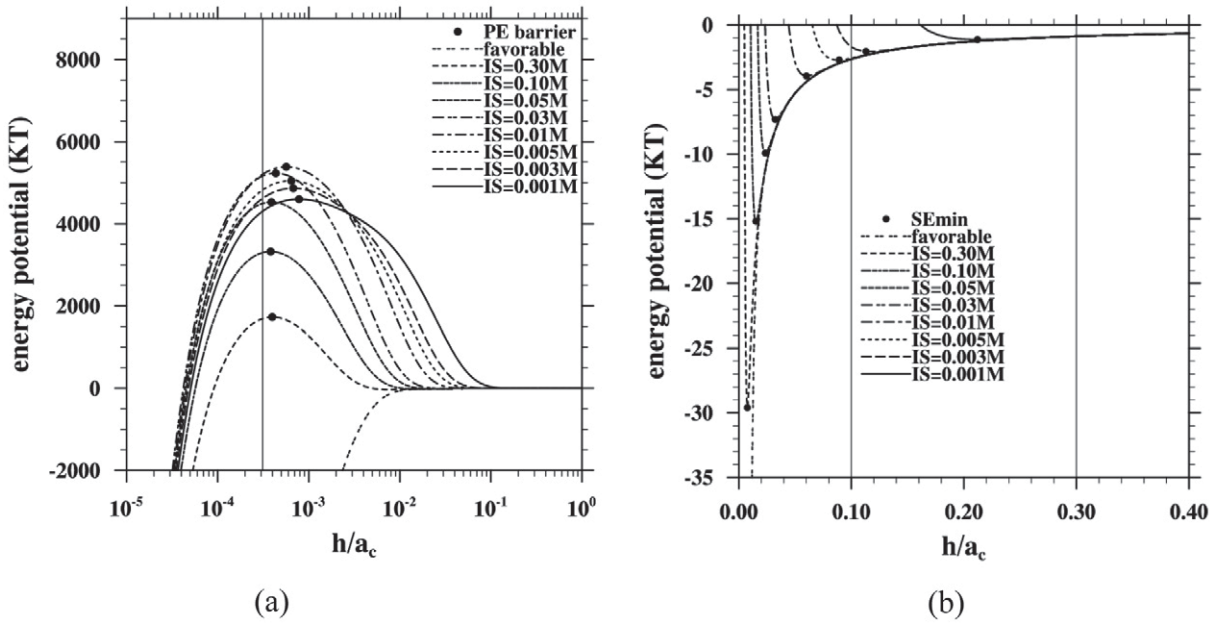

Fig. 3. Energy profiles under different solution and surface conditions: (a) profiles near the repulsive primary energy (PE) barrier; and (b) profiles near the secondary energy minimum (SEmin). The filled circles in (a) mark the peak of the repulsive energy barrier and the vertical line in (a) denotes gap distance h = equilibrium distance h_0 (Eq. [A9]) = 0.157 nm ($h/a_c = 3.14 \times 10^{-4}$, where a_c is the colloid radius). The filled circles in (b) mark the SEmin locations. Two vertical lines in (b) at a gap distance of 50 nm ($h/a_c = 0.10$) and 150 nm ($h/a_c = 0.30$) show threshold distances used to define the SEmin retention; 50 nm is the distance used to specify SEmin retention for ionic strengths (IS) of 0.01 mol/L and above, and 150 nm is used for SEmin retention at IS below 0.01 mol/L.

The total DLVO energy profiles are plotted in Fig. 3. For the conditions considered here, the repulsive energy barrier is located very close to the collector surface. For the higher ionic strength cases, it is rather close to the equilibrium distance h_0 (0.157 nm) where physical contact is assumed to occur (the vertical line drawn in Fig. 3a). Figure 3b shows that, for different ionic strengths, the energy profiles immediately outside the SEmin overlap. This is because, outside the SEmin region, the van der Waals force dominates the net DLVO force. The repulsive energy barrier height, the SEmin depth and location, and the double layer thickness for the physical conditions studied are shown in Table 3. In general, the calculated repulsive energy barrier height and the gap distance where the SEmin occurred both decrease as the solution ionic strength increases. The high values of the energy barrier imply that it is not possible for colloids to overcome this barrier. For very low ionic strength (IS < 0.03 mol/L), the energy barrier between a suspended colloid and a glass surface increases slightly with increasing ionic strength as a result of the initial increase in the ζ potential of the colloid (Table 1). On the other hand, as the solution ionic strength further increases, the SEmin depth also increases, indicating that colloids could be retained at SEmin. Indeed, these general physical scenarios will be predicted quantitatively by our model simulations.

Model Simulation: Effect of Flow Speed on Colloid Retention

In the simulation, no colloids were found to overcome the repulsive energy barrier and deposit in the primary energy minimum.

Table 3. Maximum energy barrier (Φ_{max}), secondary energy minimum (Φ_{min}) and corresponding separation distance at the secondary energy minimum (d), electrical double layer thickness ($1/\kappa$) between colloids and glass beads, and the gap distance S (and DLVO energy Φ_S) used to identify retention at the secondary energy minimum at different ionic strengths (I).

I	Φ_{max}	Φ_{min}	d	$1/\kappa$ (nm)	S (Φ_S)
mol/L	kT		nm		nm (kT)
0.001	4600	−1.13	106	9.55	150 (−1.0)
0.003	4866	−2.05	56.5	5.56	150 (−1.0)
0.005	5045	−2.71	44.6	4.31	150 (−1.0)
0.01	5389	−3.95	30.0	3.02	50 (−2.7)
0.03	5232	−7.31	16.3	1.74	50 (−2.7)
0.05	4527	−9.92	11.8	1.35	50 (−2.7)
0.1	3324	−15.2	7.61	0.95	50 (−2.7)
0.3	1729	−29.6	3.79	0.55	50 (−2.7)

A certain fraction of colloids was found to enter the SEmin well. At any given time, a colloid was assumed to be retained if it was located within a threshold gap distance from the collector surface. Such a retained colloid could still move along the collector surface tangentially within the SEmin well region or return to the bulk flow when a strong thermal fluctuation disturbance occurred. The threshold gap distance was set to 50 nm when the solution ionic strength was 0.01 mol/L or higher. This distance corresponds to a DLVO energy of −2.7 kT (see the last column of Table 3) and is larger than the gap distance corresponding to the SEmin location

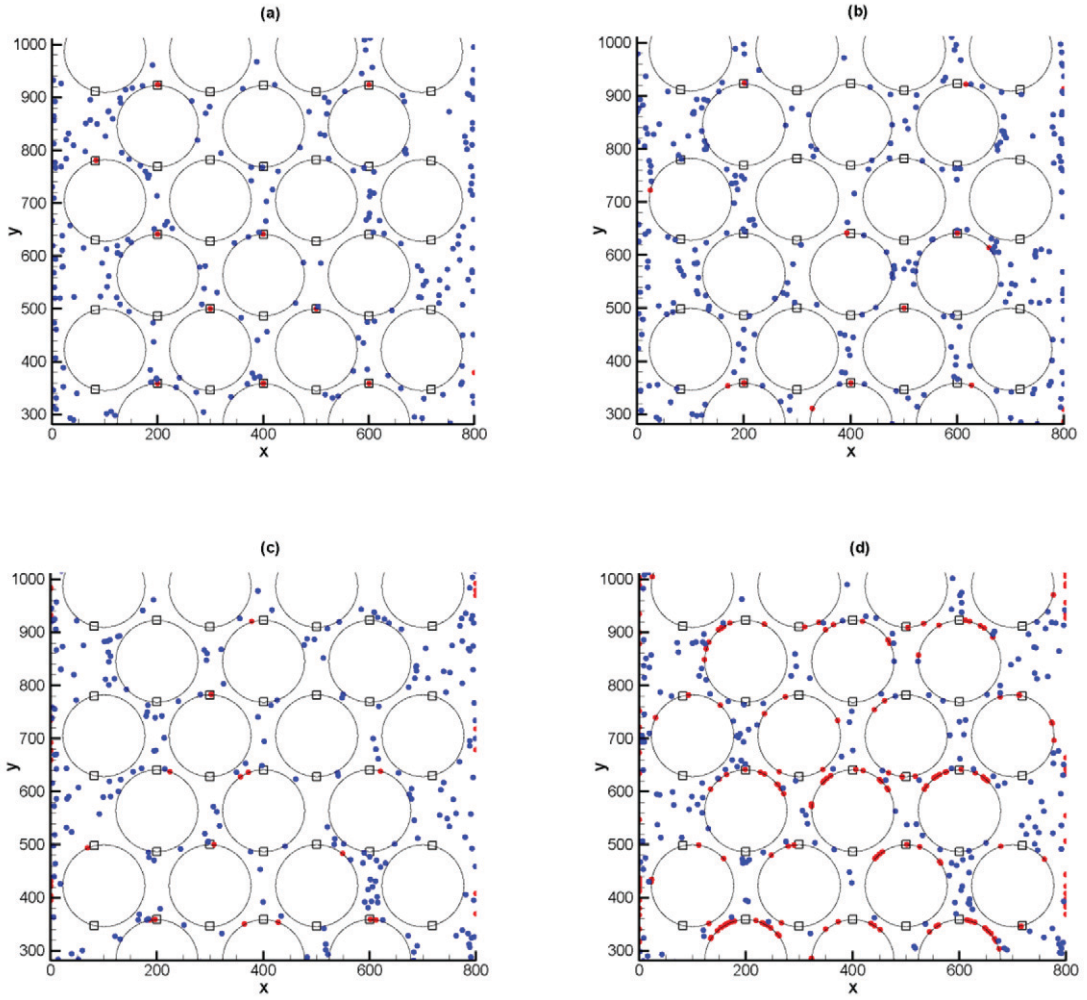

Fig. 4. Locations of colloids after injection of 6000 colloids at an interstitial velocity of (a) 0.6 mL/h or 53 m/d in 0.001 mol/L buffer solution, (b) 0.06 mL/h or 5.3 m/d in 0.001 mol/L buffer solution, (c) 0.6 mL/h or 53 m/d in 0.1 mol/L buffer solution, and (d) 0.06 mL/h or 5.3 m/d in 0.1 mol/L buffer solution. The red dots represent colloids retained at the secondary energy minimum on the glass beads or the channel walls and the blue dots represent suspended colloids. Hollow squares mark front and rear stagnation points on the glass beads. Only those colloids located in the second and third pore volumes are plotted. The unit used for the axis coordinates is 1 μm.

(see Table 3). For the lower ionic strengths (0.001, 0003, and 0.005 mol/L) considered, however, the SEmin well is shallow and is almost outside the 50-nm gap distance. In this case, the threshold location was adjusted to 150 nm. While the quantitative value of the colloid retention ratio could depend on this threshold distance, especially at low solution ionic strength, the overall conclusion to be drawn later remains unchanged.

Figure 4 shows the locations of colloids at two flow speeds and 0.1 mol/L ionic strength after 6000 colloids had been injected. These plots show the status of the colloids (suspended or retained) and their locations in the first two pore volumes. Suspended colloids are marked as blue circles and retained colloids are marked as red circles (not in scale with channel and glass bead dimensions). The number of colloids retained on the glass beads within the domain shown in Fig. 4 is 24, 31, 32, 161 for Fig. 4a, 4b, 4c, and 4d, respectively. It is clear that most colloids retained by the glass surfaces were located in the rear stagnation region or were in the process of approaching the region as a result of the slow tangential motion of retained colloids within the SEmin. The colloid retention ratio increased significantly as the ionic strength changed from 0.001 to 0.1 mol/L. Furthermore, more colloids were retained at flow speed of 5.3 than at 53 m/d.

To quantitatively compare the retention rate, we introduce surface coverage (SC), defined as the ratio of the total projection area of all the colloids retained in the SEmin to the total area of the collector surface:

$$\mathrm{SC} = \frac{\pi a_c^2 N_c}{A} \qquad [5]$$

where a_c is the colloid radius, N_c is the number of colloids retained in the SEmin and A is the total surface area of glass cylinders and

channel walls within the region from the inlet containing the same amount of solution that has been injected at the inlet. The total fluid volume injected during a time interval T can be expressed as $U_0 H a_{cyl} \alpha T$, where α is the porosity. The fluid volume in the elemental simulation domain is $\alpha H L a_{cyl}$ and the collector surface area in this domain is $2La_{cyl} + 14\pi a_{cyl}^2$. Therefore, the collector surface area A covered by the injected fluid volume can be expressed as

$$A = \left(2La_{cyl} + 14\pi a_{cyl}^2\right)\frac{U_0 H a_{cyl}\alpha T}{\alpha H L a_{cyl}} = U_0 T a_{cyl}\left(2 + 14\pi\frac{a_{cyl}}{L}\right) \quad [6]$$

In our model, $a_{cyl}/L = 0.273$, which implies that the glass cylinders contribute to 86% of the collector surface. Figure 5 shows the surface coverage as a function of the flow speed after 6000 colloids have been injected at the inlet. Ten different flow speeds from 2 to 150 m/d were considered, with the ionic strength fixed at 0.1 mol/L. To reveal the exact role of Brownian motion, results without Brownian motion are also shown. For a given number of injected colloids, the surface coverage decreased with increasing fluid speed. At lower flow speeds (<25 m/d), the surface coverage depended strongly on the flow speed, and Brownian motion was found to be the dominant mechanism for this strong dependence. More specifically, Brownian motion led to an increase in surface coverage by factor of 2 to 7 when compared with the results with Brownian motion switched off. At higher flow speeds, the overall effect of Brownian motion appears to be independent of flow speed; namely, the surface coverage including Brownian motion is roughly twice that without Brownian motion. A scaling analysis also showed that the magnitude of the Brownian force is comparable to the drag force at the critical flow speed of 25 m/d. A similar dependence of surface coverage on flow speed was shown by Unni and Yang (2005, Fig. 5) using a simple parallel plate channel as the flow passage, although they did not identify a critical flow speed.

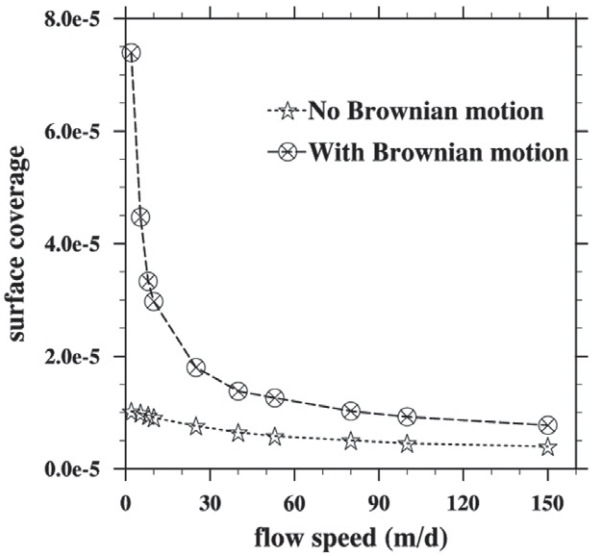

Fig. 5. Predicted surface coverage of 1-μm sulfate latex colloids at different flow speeds at an ionic strength of 0.1 mol/L after 6000 colloids have been injected at the inlet.

We must point out that the critical flow speed noted here is very different from the critical flow speed studied in Shen et al. (2010), who showed that, for a similar colloid size (~1 μm), there exists a critical flow speed (~0.05 m/d) below which the attachment efficiency is independent of the flow speed. While we did not study such a low flow speed range here, Fig. 5 does imply that Brownian motion will control the retention when the flow speed is significantly less than 1 m/d.

Physically, the effect of flow speed on colloidal retention is determined by the balance between transport by hydrodynamic drag force and interaction with the collector surface via Brownian and colloidal forces. These forces depend on the distance from the collector surface and the fluid chemistry. Hydrodynamic drag and Brownian forces dominate in the majority of the domains, while colloidal forces are only important in the vicinity of the collector surfaces. The drag force increases with the flow speed, leading to a higher colloid transport velocity that decreases the transit or residence time of suspended colloids. While the drag force moves suspended particles along the streamlines that are nearly tangential to the surface of the glass cylinders or channel walls, the random motion due to the Brownian force tends to shift colloids across the streamlines. The cumulative effect of Brownian motion on a colloid trajectory increases with the residence time of a colloid within a given pore volume. Therefore, the Brownian force plays a relatively more significant role at lower flow speeds because of the relatively longer residence time. At sufficiently short separation distances near the SEmin well, the attractive van der Waals force can drive the colloid toward the SEmin region. In regions very close to collectors, Brownian motion could play a more significant role than the hydrodynamic drag because of the very low fluid velocities.

This competing effect between Brownian motion and convective transport is illustrated further in Fig. 6, where we compare the distribution of the injection locations of those colloids retained by a collector surface. Namely, for each retained colloid, we trace them back to their initial injection location at the inlet with and without Brownian motion. When the flow speed is low, colloids have to be injected at specific locations to approach a collector surface without Brownian motion (Fig. 6a), while with Brownian motion, colloids injected at almost all locations in the bulk solution at the inlet could reach a collector (Fig. 6c). At the higher flow speed, the effect of Brownian diffusion is less significant, as shown by the very spiky distribution at the inlet (Fig. 6b and 6d). This explains why the surface coverage is very sensitive to the flow speed when the speed is <25 m/d (Fig. 5).

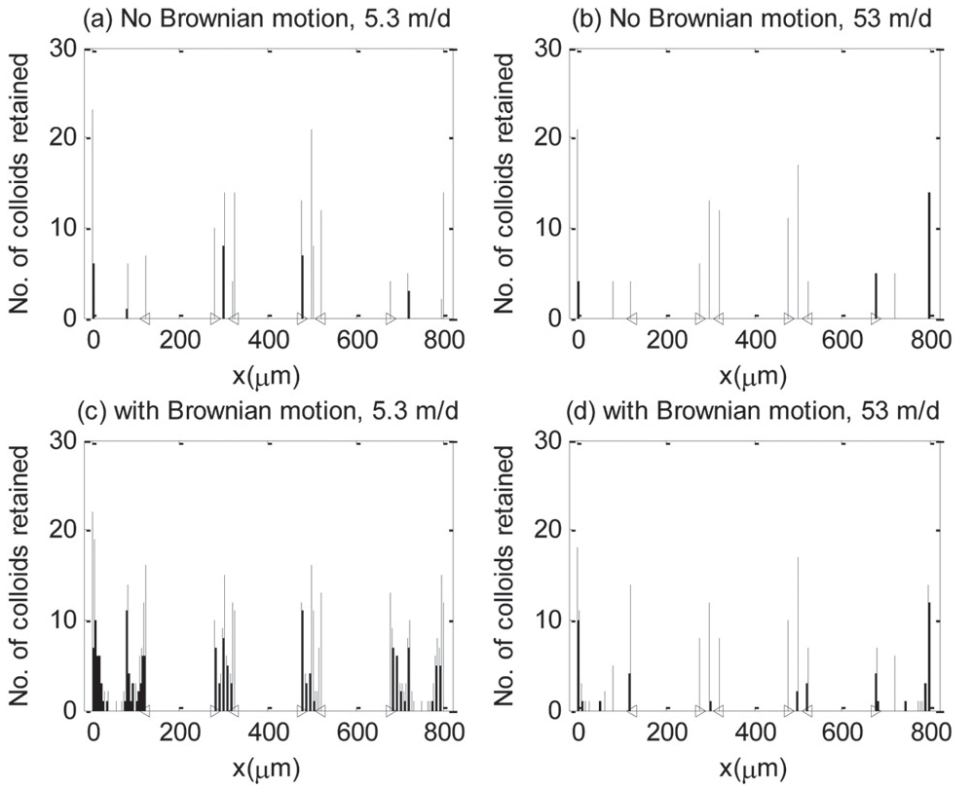

Fig. 6. The distribution of injection locations for those colloids retained by the channel walls and the glass beads when 6000 colloids had been injected: (a) no Brownian motion at 5.3 m/d, (b) no Brownian motion at 53 m/d, (c) with Brownian at 5.3 m/d, (d) with Brownian motion at 53 m/d. Eight hundred bins were used.

Flow speed also affects colloid retention by changing the hydrodynamic force and torque through local flow shear near a collector surface, leading to reduced retention (Yiantsios and Karabelas 2003). The local shear rate increases with increasing fluid velocity. Torque and lift associated with shear flow might also drive reentrainment of colloids that are not strongly attached on collector surfaces (i.e., via secondary-minimum retention; see Bradford and Toride, 2007; Torkzaban et al., 2007). The exact force and torque formulation in this case, however, is still debated (Johnson et al., 2009; Torkzaban et al., 2009). These aspects were not considered in our simulations and uncertainties remain.

Model Simulation: Effect of Ionic Strength on Colloid Retention

Figure 7 compares surface coverages for various ionic strengths at a flow speed of 8 m/d. Surface coverage increased with increasing ionic strength until it reached saturation; namely, any further increase in ionic strength would no longer change the surface coverage. The saturated surface coverage was achieved at an ionic strength close to 0.01 mol/L, which corresponds to a SEmin depth of −4 kT (Table 3) in our numerical simulations. At low ionic strengths, the surface coverage was smaller and at the same time showed increasing fluctuations as the ionic strength was reduced, representing the stochastic nature of retention by the SEmin associated with a lower probability of capture.

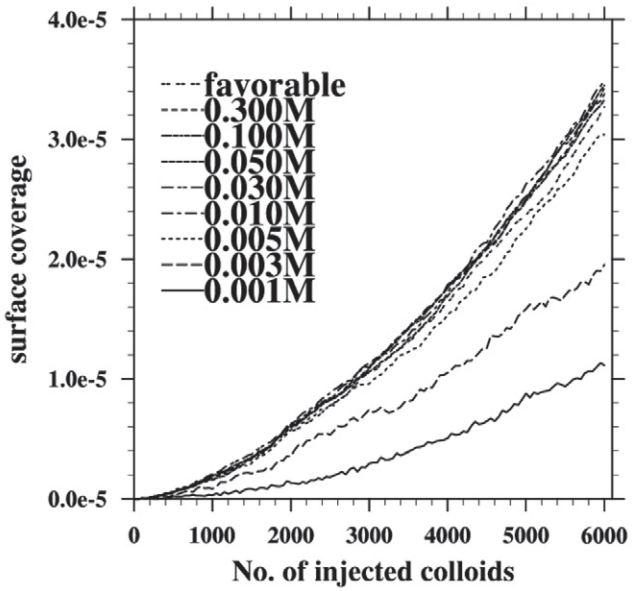

Fig. 7. Surface coverage of 1-μm sulfate latex colloids at different ionic strengths at a flow speed of 8 m/d. All colloids were retained at the secondary energy minimum. In addition, surface coverage for a favorable condition is plotted for comparison (with attractive electrostatic force that matches the magnitude of the repulsive electrostatic force for our 0.1 mol/L case). For this favorable condition, colloids were deposited at the primary energy minimum.

This saturation is consistent with the fact that the thermal energy of colloids is not likely to exceed −4 kT according to the Maxwell model for thermal fluctuations first proposed by Maxwell in 1859 (Kubo, 1966). Namely, when the SEmin well is deep enough, colloids cannot escape the SEmin well once they are captured. The amount of colloids that can be driven into the near-surface region, however, is not determined by the solution ionic strength but rather by the competition of the hydrodynamic transport along the streamline and Brownian cross-streamline shifting. This is because (i) the energy profiles outside the SEmin region overlap for different ionic strengths (Fig. 3b) and (ii) the net colloidal force is negligible outside the SEmin region when compared with the hydrodynamic and Brownian forces. These explain why saturation must occur with increasing ionic strength for a prescribed flow speed. Therefore, the effect of ionic strength on colloid retention (and virus removal) seems to be only important below a certain threshold value, beyond which changes in ionic strength have little impact on colloid transport and retention. This can be seen by comparing the results for ionic strengths of 0.01 and 0.3 mol/L in Fig. 7. The −4 kT interaction energy found in our simulations agrees well with the Maxwell model prediction by Shen et al. (2007, Fig. 1a). The modeling results are also consistent with experimental observations of virus removal in response to changes in ionic strength in previous studies (Chu et al., 2000; Thompson et al., 1998; Penrod et al., 1996). Thompson et al. (1998) found that removal of bacteriophage MS-2 was not affected by solution ionic strength at electrolyte concentrations <0.03 mol/L but increased rapidly with increasing ionic strength between 0.03 and 0.1 mol/L and increased slowly above 0.1 mol/L. In column experiments where the solution ionic strength was continuously increased, Chu et al. (2000) found that the removal of MS-2 was sensitive to ionic strength changes only in the range between 0.03 and 0.1 mol/L. The phenomenon that removal of viruses seems to be affected by solution ionic strength within a range bounded by certain critical or threshold values has also been observed for other types of colloids (Penrod et al., 1996).

Comparison of Model Predictions with Microscopic Observations

Results from the confocal visualization experiments with sulfate-latex microspheres at flow rates of 0.06 and 0.6 mL/h (interstitial velocity of 5.3 and 53 m/d, respectively) at ionic strengths of 0.001 and 0.1 mol/L are shown in Fig. 8. To be consistent with the model simulations, confocal images were taken after the same pore volume of colloidal suspension had flowed through the focused area. The images in Fig. 8 show the distribution of colloids after approximately 0.1 mL of colloidal suspension had moved through the observation area. There was very little colloid deposition in 0.001 mol/L buffer solution at a flow rate of 0.6 mL/h (Fig. 8a), which is consistent with the simulation results under the same physicochemical conditions. As the flow rate was reduced to 0.06 mL/h, more retained colloids were observed on glass beads (Fig.

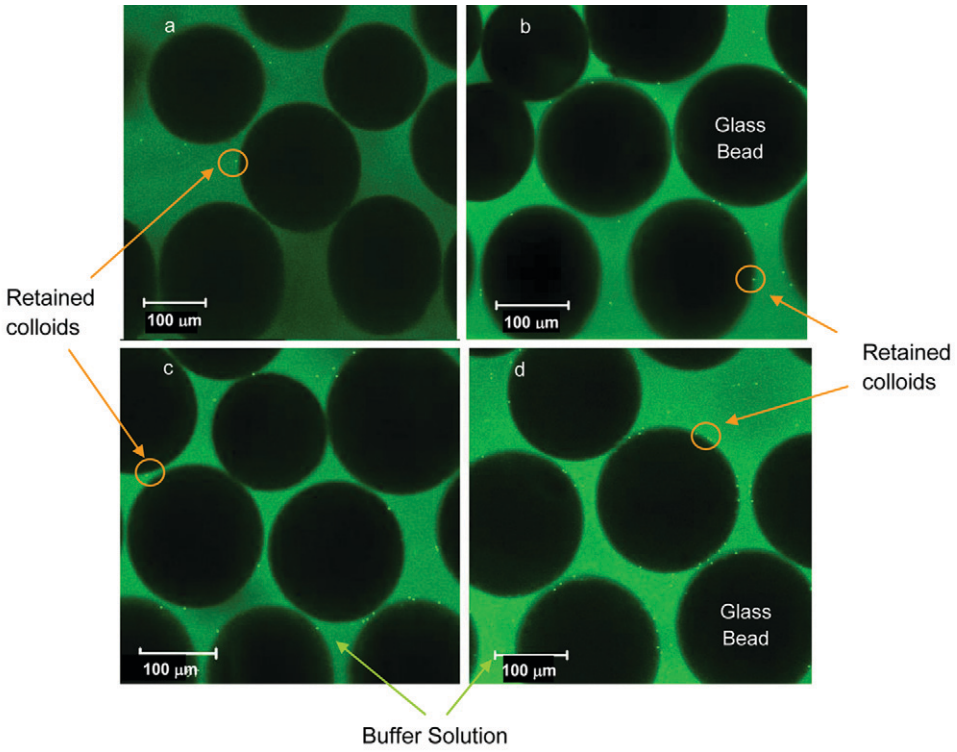

Fig. 8. Visualization of retained colloids at two different flow rates and two different ionic strengths: (a) 0.6 mL/h or 53 m/d in 0.001 mol/L buffer solution, (b) 0.06 mL/h or 5.3 m/d in 0.001 mol/L buffer solution, (c) 0.6 mL/h or 53 m/d in 0.1 mol/L buffer solution, and (d) 0.06 mL/h or 5.3 m/d in 0.1 mol/L buffer solution. The mean flow is from left to right.

8b). The number of deposited colloids increased significantly as the solution ionic strength increased to 0.1 mol/L (Fig. 8c and 8d). The same trend was observed in the model simulations: a much larger number of colloids were retained at glass bead surfaces at an ionic strength of 0.1 mol/L than at 0.001 mol/L, especially at the flow speed of 5.3 m/d. While the general results are qualitatively similar, there are some quantitative discrepancies between the model results and the pore-scale experimental observations. This is to be expected for several possible reasons. First, unlike the assumption for the model calculations that collectors have uniform surface properties and are smooth, the glass beads used in the micromodel experiments may not have been perfect spheres and may have had a certain degree of surface roughness as well as surface charge heterogeneity. Some colloids may experience net attractive force or hydrophobic interaction due to surface heterogeneity. Surface roughness may produce a stronger friction and distribution of adhesive torque on the colloids, which can prevent reentrainment of a portion of the deposited colloids. Second, while the two-dimensional model simulation captures the essential features of the experimental system, it is unlikely to completely represent the three-dimensional flow and all the geometric features. For example, colloids strained at grain–grain contacts can occur in the three-dimensional micromodel and can contribute to colloid retention in saturated porous media (Bradford et al., 2003, 2007; Johnson et al., 2007).

Concluding Remarks

In this study, we developed a two-dimensional simulation model to study the transport and retention of colloids in saturated porous media under unfavorable surface conditions. Despite the limitations associated with the two-dimensional model, it provides mechanistic insights for improved understanding of colloid retention and transport processes and how these processes are affected by relevant parameters. Given the large range of length and time scales involved in a pore-scale trajectory based approach, a two-dimensional simulation model does have the unique advantage of covering different physical conditions (here, different flow speeds and ionic strengths) in a computationally efficient manner. In this regard, the two-dimensional model developed here could continue to serve as a qualitative and semiquantitative mechanistic research tool. The successful simulation of the ionic strength effects on the complex retention behavior of amphiphilic colloids shows that this computational approach does properly capture the physical effects of pore-scale hydrodynamic and colloid–surface interactions. Conducting experiments to quantify the retention of biocolloids such as viruses across a wide range of ionic strengths with sufficient detail is very labor intensive and the large errors involved in virus assays compromises our ability to obtain the results needed for accurate analysis. The modeling exercise presented in this study significantly improves our ability to tackle such research problems.

The simulation results led to the following mechanistic insights into colloid retention at the SEmin. The fraction of colloids that can move into the SEmin well, where the attractive van der Waals force operates to retain the colloids, is controlled by the competition of hydrodynamic transport along the streamline and Brownian shifting across the streamline. Once a colloid is retained, it could continue to drift slowly toward the rear stagnation region along the surface due to the tangential hydrodynamic force, causing the accumulation of retained colloids near the rear stagnation region. This is consistent with previous experimental observations (i.e., Kuznar and Elimelech, 2007) and numerical results (Johnson et al., 2007). Retention was found to be dynamically irreversible when the SEmin depth reached about −4 kT. Furthermore, for a given ionic strength, a critical flow speed was found below which Brownian motion dominated the retention rate, leading to a strong dependence of surface coverage on the flow velocity. This competing effect between Brownian motion and convective transport was also demonstrated by examining the distribution of the injection locations of the retained colloids.

The model developed in our study provides a useful framework that can be systematically made more complex and accurate by including factors and physical processes not considered in this study. Recently, we have extended the model to three-dimensional porous media (Gao et al., 2010). The Lagrangian trajectory approach allows consideration of chemical and physical heterogeneities, such as charge variations and surface roughness. A systematic incorporation of these factors and additional processes into our simulation model will ultimately improve our understanding and ability to predict colloid retention and transport in natural soil and groundwater aquifers.

Appendix

Formulation of Forces Acting on a Colloid

The hydrodynamic drag forces in the normal and tangential directions were calculated as

$$F_{i,\mathrm{n}}^{\mathrm{drag}} = \xi\left(f_2 u_{i,\mathrm{n}} - \frac{V_{i,\mathrm{n}}}{f_1}\right)$$
$$F_{i,\mathrm{t}}^{\mathrm{drag}} = \frac{\xi}{f_4}\left(f_3 u_{i,\mathrm{t}} - V_{i,\mathrm{t}}\right) \qquad [A1]$$

where $u_{i,\mathrm{n}}$ and $u_{i,\mathrm{t}}$ (m/s) are the fluid velocities in the normal and tangential directions, respectively, $\xi \equiv 6\pi\mu a_c$, μ is the fluid viscosity and a_c is the colloid radius. The hydrodynamic correction factors, f_1 to f_4, account for the modification of the hydrodynamic force due to the presence of a surface, and they are a function of the nondimensional gap distance $\overline{h} = h/a_c$, where h is the gap distance. These correction factors were discussed in the literature (Brenner, 1961; Goldman et al., 1967; Goren 1970; Goren and O'Neill, 1971; Spielman and Fitzpatrick, 1973; Heimenz and

Rajagopalan, 1997). The specific functional forms used here were given in Gao et al. (2010). The Stokes relaxation time of a colloid, τ_p (s), is defined as

$$\tau_p = \frac{m_c}{6\pi\mu a_c} = \frac{2\rho_c a_c^2}{9\mu} \quad [A2]$$

where ρ_c = 1055 kg/m^3 is the colloid density. An important parameter characterizing the dynamic response of a colloid to the flow is the Stokes number, St, the ratio of the Stokes relaxation time to the characteristic time of flow:

$$St = \frac{\tau_p U_0}{D_g} \quad [A3]$$

where U_0 is the interstitial flow velocity (defined as the volume flow rate over the product of channel cross-sectional area and porosity) and D_g is the diameter of the grain particles. For the current application, we found that St $\sim 2.09 \times 10^{-8}$ when U_0 = 5 m/d, implying that colloids would essentially follow the flow streamlines if colloidal forces and Brownian motion were not considered. Note that the effect of the added mass, although not explicitly considered here, does not change this condition. Thus, colloids are essentially inertialess particles in our simulations.

The colloidal force term includes electrostatic (EDL), Lifshitz–van der Waals (LW), and Lewis acid–base (AB) interaction forces (van Oss, 1994). Each interaction force acts in the direction normal to a surface, with a positive value indicating a repulsive force and a negative value an attractive force. The formulation of these forces is primarily based on DLVO interaction potential (Derjaguin and Landau, 1941; Verwey and Overbeek, 1948). The total colloidal force was obtained as

$$F_{i,n}^{C} = -\frac{d\Phi_i^{EDL}}{dh} - \frac{d\Phi_i^{LW}}{dh} - \frac{d\Phi_i^{AB}}{dh} \quad [A4]$$

The electrostatic double layer interaction energy Φ_i^{EDL} between a colloid and glass surface was calculated as (Hogg et al., 1966)

$$\Phi_i^{EDL} = \pi\varepsilon_0\varepsilon_r a_c \left\{ 2\psi_s\psi_c \ln\left[\frac{1+\exp(-\kappa h)}{1-\exp(-\kappa h)}\right] + \left(\psi_s^2 + \psi_c^2\right)\ln\left[1-\exp(-2\kappa h)\right]\right\} \quad [A5]$$

where ε_0 is the dielectric permittivity in a vacuum and equals to 8.85×10^{-12} C^2/(J m), ε_r is the dielectric constant of the medium, and for water at 298 K, ε_r = 78.54 (dimensionless), κ (1/m) is the inverse Debye length, and ψ_s (V) and ψ_c (V) are the surface potentials of the glass surface and colloid, respectively. The electrostatic double layer interaction between suspended colloids and deposited colloids was computed as (Elimelech et al., 1995)

$$\Phi_i^{EDL} = 32\pi\varepsilon_0\varepsilon_r a_c \left(\frac{kT}{Ze}\right)^2 \times \left[\tanh\left(\frac{Ze\psi_c}{4kT}\right)\right]^2 \exp(-\kappa h) \quad [A6]$$

where k (J/K) is the Boltzmann constant (1.38×10^{-23} J/K), T (K) is the absolute temperature, e is the charge on an electron (1.6×10^{-19} C), and Z is the valence.

The surface potentials of the colloid (ψ_c) and glass bead surface (ψ_s) were derived by

$$\psi_c = \zeta_c\left(1+\frac{z}{a_c}\right)e^{\kappa z}$$
$$\tanh\left(\frac{Ze\psi_s}{4kT}\right) = \tanh\left(\frac{Ze\zeta_s}{4kT}\right)e^{\kappa z} \text{ or } \psi_s \sim \zeta_s \exp(\kappa z) \quad [A7]$$

where ζ_c (V) and ζ_s (V) are the ζ potentials of the colloid and glass surface, respectively, measured at the slipping plane by electrokinetic methods, and z (m) is the distance from the particle surface to the slipping plane, a distance that is generally on the order of 3 to 5 Å (Liang et al., 2007). A value of 5 Å was used in the calculations performed in this study. The thickness of the electrostatic double layer, or Debye length, is defined as

$$\frac{1}{\kappa} = \left(\frac{\varepsilon_0\varepsilon_r kT}{e^2 N_A \sum_i Z_i^2 M_i}\right)^{1/2} \quad [A8]$$

where N_A is Avogadro's number (6.02×10^{23} ions/mol), Z_i (dimensionless) is the valence of the ith ionic species, and M_i (mol/m^3) is the molar concentration of the ith ionic species.

The Lifshitz–van der Waals free energy accounts for intermolecular interactions including London dispersion, Keesom dipole–dipole, and Debye induction. It was calculated as (van Oss, 1994)

$$\Phi_i^{LW} = -4\pi\frac{h_0^2}{h}a_c\left(\sqrt{\gamma_3^{LW}} - \sqrt{\gamma_2^{LW}}\right)\left(\sqrt{\gamma_3^{LW}} - \sqrt{\gamma_1^{LW}}\right) \quad [A9]$$

where h_0 [m] is the equilibrium distance set to 1.57×10^{-10} m, where physical contact between a colloid and cylinder surface occurs, χ is the water decay length set to 0.6 nm (van Oss, 1994), γ^{LW} (J/m^2) is the Lifshitz–van der Waals component of the surface tension, with 1 denoting a colloid, 2 denoting glass, and 3 denoting water.

Finally, Lewis acid–base interaction originates from the bonding reaction of a Lewis acid and a Lewis base. The interaction energy was expressed as (Liang et al., 2007)

$$\Phi_i^{\mathrm{AB}} = -4\pi h_0 a_c \exp\left(\frac{h_0 - h}{\chi}\right) \times\left[\sqrt{\gamma_3^+}\left(\sqrt{\gamma_1^-}+\sqrt{\gamma_2^-}-\sqrt{\gamma_3^-}\right) +\left(\sqrt{\gamma_3^-}\left(\sqrt{\gamma_1^+}+\sqrt{\gamma_2^+}-\sqrt{\gamma_3^+}\right) -\sqrt{\gamma_1^+\gamma_2^-}-\sqrt{\gamma_1^-\gamma_2^+}\right]\right. \quad [A10]$$

where γ^+ (J/m^2) is the electron-acceptor parameter and γ^- (J/m^2) is the electron-donor parameter of the Lewis acid–base component of surface tension.

The solution was modeled as a continuum. Because the colloids are small, their motion is affected by the Brownian motion or thermal fluctuations of solvent molecules. At each time step, this Brownian fluctuating motion is modeled separately by adding the following velocity increments in the normal and tangential directions, respectively:

$$m_c \mathrm{d}V_{i,\mathrm{n}} = F_{i,\mathrm{n}}^{\mathrm{B}}\mathrm{d}t$$
$$m_c \mathrm{d}V_{i,\mathrm{t}} = F_{i,\mathrm{t}}^{\mathrm{B}}\mathrm{d}t \quad [A11]$$

$$F_{i,\mathrm{n}}^{\mathrm{B}} = \xi\sqrt{\frac{2D_0}{f_1 \mathrm{d}t}}G(0,1)$$
$$F_{i,\mathrm{t}}^{\mathrm{B}} = \xi\sqrt{\frac{2D_0}{f_4 \mathrm{d}t}}G(0,1) \quad [A12]$$

where the diffusivity in the bulk solution is $D_0 = kT/\xi$, $G(0,1)$ represents a Gaussian distribution whose mean is zero and standard deviation is 1, and dt (s) is the time step size. It should be noted that the local hydrodynamic interaction reduces the diffusion coefficient in the normal and tangential directions by a factor of f_1 and f_4, respectively.

Acknowledgments

This project was supported by the USDA (NRI 2006-02551 and NRI 2008-02803) and the U.S. National Science Foundation (CBET-0932686). We thank Dr. Kirk Czymmek at the Bio-imaging Center at the University of Delaware for providing training and support for the confocal experiment. Computing resources were provided by the National Center for Atmospheric Research through CISL-35751010, CISL-35751014, and CISL-35751015.

References

Berry, R.A., R.C. Martineau, and T.R. Wood. 2004. Particle-based direct numerical simulation of contaminant transport and deposition in porous flow. Vadose Zone J. 3:164–169. doi:10.2113/3.1.164

Bradford, S.A., J. Šimůnek, M. Bettahar, M.Th. van Genuchten, and S.R. Yates. 2003. Modeling colloid attachment, straining, and exclusion in saturated porous media. Environ. Sci. Technol. 37:2242–2250. doi:10.1021/es025899u

Bradford, S.A., and N. Toride. 2007. A stochastic model for colloid transport and deposition. J. Environ. Qual. 36:1346–1356. doi:10.2134/jeq2007.0004

Bradford, S.A., S. Torkzaban, and S.L. Walker. 2007. Coupling of physical and chemical mechanisms of colloid straining in saturated porous media. Water Res. 41:3012–3024. doi:10.1016/j.watres.2007.03.030

Brenner, H. 1961. The slow motion of a sphere through a viscous fluid towards a plane surface. Chem. Eng. Sci. 16:242–251. doi:10.1016/0009-2509(61)80035-3

Burganos, V.N., A.C. Michalopoulou, G. Dassios, and A.C. Payatakes. 1992. Creeping flow around and through a permeable sphere moving with constant velocity towards a solid wall: A revision. Chem. Eng. Commun. 117:85–88. doi:10.1080/00986449208936058

Burganos, V.N., C.A. Paraskeva, P.D. Christofides, and A.C. Payatakes. 1994. Motion and deposition of non-Brownian particles in upflow collectors. Sep. Technol. 4:47–54. doi:10.1016/0956-9618(94)80005-7

Chen, G., and M. Flury. 2005. Retention of mineral colloids in unsaturated porous media as related to their surface properties. Colloid Surf. A 256:207–216. doi:10.1016/j.colsurfa.2005.01.021

Chen, G., M. Flury, J.B. Harsh, and P.C. Lichtner. 2005. Colloid-facilitated transport of cesium in variably saturated Hanford sediments. Environ. Sci. Technol. 39:3435–3442. doi:10.1021/es048978+

Chen, S., and G. Doolen. 1998. Lattice Boltzmann method for fluid flows. Annu. Rev. Fluid Mech. 30:329–364. doi:10.1146/annurev.fluid.30.1.329

Chu, Y., Y. Jin, and M.V. Yates. 2000. Virus transport through saturated sand columns as affected by different buffer solutions. J. Environ. Qual. 29:1103–1110. doi:10.2134/jeq2000.00472425002900040010x

Crist, J.T., J.F. McCarthy, Y. Zevi, P. Baveye, J.A. Throop, and T.S. Steenhuis. 2004. Pore-scale visualization of colloid transport and retention in partly saturated porous media. Vadose Zone J. 3:444–450.

Crist, J.T., Y. Zevi, J.F. McCarthy, J.A. Throop, and T.S. Steenhuis. 2005. Transport and retention mechanisms of colloids in partially saturated porous media. Vadose Zone J. 4:184–195.

Cushing, R.S., and D.F. Lawler. 1998. Depth filtration: Fundamental investigation through three-dimensional trajectory analysis. Environ. Sci. Technol. 32:3793–3801. doi:10.1021/es9707567

Derjaguin, B.J., and L. Landau. 1941. Theory of the stability of strongly charged lyophobic sols and of the adhesion of strongly charged particles in solutions of electrolytes. Acta Physicochim. URSS 14:633–662.

Elimelech, M., J. Gregory, X. Jia, and R. Williams. 1995. Particle deposition and aggregation: Measurement, modeling and simulation. Butterworth-Heinemann, Boston.

Elimelech, M., and C.R. O'Melia. 1990a. Effect of particle size on collision efficiency in the deposition of Brownian particles with electrostatic energy barriers. Langmuir 6:1153–1163. doi:10.1021/la00096a023

Elimelech, M., and C.R. O'Melia. 1990b. Kinetics of deposition of colloidal particles in porous media. Environ. Sci. Technol. 24:1528–1536. doi:10.1021/es00080a012

Elimelech, M., and C.R. O'Melia. 1990c. Effect of electrolyte type on the electrophoretic mobility of polystyrene latex colloids. Colloids Surf. 44:165–177. doi:10.1016/0166-6622(90)80194-9

Gao, H., J. Han, Y. Jin, and L.-P. Wang. 2008. Modeling microscale flow and colloid transport in saturated porous media. Int. J. Comput. Fluid Dyn. 22:493–505. doi:10.1080/10618560802238259

Gao, H., C.Q. Qiu, D. Fan, Y. Jin, and L.-P. Wang. 2010. Three-dimensional microscale flow simulation and colloid transport modeling in saturated soil porous media. Comput. Math. Appl. 59:2271–2289. doi:10.1016/j.camwa.2009.08.057

Goldman, A.J., R.G. Cox, and H. Brenner. 1967. Slow viscous motion of a sphere parallel to a plane wall: I. Motion through a quiescent fluid. Chem. Eng. Sci. 22:637–653. doi:10.1016/0009-2509(67)80047-2

Goren, S.L. 1970. Normal force exerted by creeping flow on a small sphere touching a plane. J. Fluid Mech. 41:619–625. doi:10.1017/S0022112070000782

Goren, S.L., and M.E. O'Neill. 1971. Hydrodynamic resistance to a particle of a dilute suspension when in the neighbourhood of a large obstacle. Chem. Eng. Sci. 26:325–338. doi:10.1016/0009-2509(71)83008-7

Grolimund, D., and M. Borkovec. 2005. Colloid-facilitated transport of strongly sorbing contaminants in natural porous media: Mathematical modeling and laboratory column experiments. Environ. Sci. Technol. 39:6378–6386. doi:10.1021/es050207y

Hahn, M.W., D. Abadzic, and C.R. O'Melia. 2004. Aquasols: On the role of secondary minima. Environ. Sci. Technol. 38:5915–5924. doi:10.1021/es049746d

Hahn, M.W., and C.R. O'Melia. 2004. Deposition and reentrainment of Brownian particles in porous media under unfavorable chemical conditions: Some concepts and applications. Environ. Sci. Technol. 38:210–220. doi:10.1021/es030416n

Han, J., Y. Jin, and C.W. Wilson. 2006. Virus retention and transport in chemically heterogeneous porous media under saturated and unsaturated flow conditions. Environ. Sci. Technol. 40:1547–1555. doi:10.1021/es051351m

Happel, J. 1958. Viscous flow in multiparticle systems: Slow motion of fluids relative to beds of spherical particles. AIChE J. 4:197–201. doi:10.1002/aic.690040214

Heimenz, P.C., and R. Rajagopalan. 1997. Principles of colloid and surface chemistry. Marcel Dekker, New York.

Hogg, R., T.W. Healy, and D.W. Fuerstenau. 1966. Mutual coagulation of colloidal dispersions. Trans. Faraday Soc. 62:1638–1651. doi:10.1039/tf9666201638

Johnson, W.P., X. Li, M. Tong, and H. Ma. 2009. Comment on "Transport and fate of bacteria in porous media: Coupled effects of chemical conditions and pore space geometry" by Saeed Torkzaban et al. Water Resour. Res. 45:W09603. doi:10.1029/2008WR007389

Johnson, W.P., X. Li, and G. Yal. 2007. Colloid retention in porous media: Mechanistic confirmation of wedging and retention in zones of flow stagnation. Environ. Sci. Technol. 41:1279–1287. doi:10.1021/es061301x

Kretzschmar, R., M. Borkovec, D. Grolimund, and M. Elimelech. 1999. Mobile subsurface colloids and their role in contaminant transport. Adv. Agron. 66:121–193. doi:10.1016/S0065-2113(08)60427-7

Kubo, R. 1966. Fluctuation–dissipation theorem. Rep. Prog. Phys. 29:255. doi:10.1088/0034-4885/29/1/306

Kuznar, Z.A., and M. Elimelech. 2007. Direct microscopic observation of particle deposition in porous media: Role of the secondary energy minimum. Colloids Surf. A 294:156–162. doi:10.1016/j.colsurfa.2006.08.007

Lazouskaya, V., Y. Jin, and D.J. Or. 2006. Interfacial interactions and colloid retention under steady flows in a capillary channel. Colloid Interface Sci. 303:171–184. doi:10.1016/j.jcis.2006.07.071

Li, X., Z. Li, and D. Zhang. 2010. Role of low flow and backward flow zones on colloid transport in pore structures derived from real porous media. Environ. Sci. Technol. 44:4936–4942. doi:10.1021/es903647g

Liang, Y., N. Hilal, P. Langston, and V. Starov. 2007. Interaction forces between colloidal particles in liquid: Theory and experiment. Adv. Colloid Interface Sci. 134–135:151–166. doi:10.1016/j.cis.2007.04.003

Long, W., and M. Hilpert. 2008. Lattice-Boltzmann modeling of contaminant degradation by chemotactic bacteria: Exploring the formation and movement of bacterial bands. Water Resour. Res. 44:W09415. doi:10.1029/2007WR006129

Long, W., and M. Hilpert. 2009. A correlation for the collector efficiency of Brownian particles in clean-bed filtration in sphere packings by a lattice-Boltzmann method. Environ. Sci. Technol. 43:4419–4424. doi:10.1021/es8024275

Long, W., H. Huang, J. Serlemitsos, E. Liu, A.H. Reed, and M. Hilpert. 2010. Pore-scale study of the collector efficiency of nanoparticles in packings of nonspherical collectors. Colloids Surf. A 358:163–171. doi:10.1016/j.colsurfa.2010.01.043

McCarthy, J.F., and J.M. Zachara. 1989. Subsurface transport of contaminants: Mobile colloids in the subsurface environment may alter the transport of contaminants. Environ. Sci. Technol. 23:496–502.

Overbeek, J.T.G. 1952. Electrokinetics. p. 194–244. In H. Kruyt (ed.) Colloid science. Elsevier, Amsterdam.

Paraskeva, C.A., V.N. Burganos, and A.C. Payatakes. 1991. Three-dimensional trajectory analysis of particle deposition in constricted tubes. Chem. Eng. Commun. 108:23–48. doi:10.1080/00986449108910949

Payatakes, A.C., R. Rajagopalan, and C. Tien. 1974a. Application of porous media models to the study of deep bed filtration. Can. J. Chem. Eng. 52:722–731.

Payatakes, A.C., C. Tien, and R.M. Turian. 1974b. Trajectory calculation of particle deposition in deep bed filtration: 1. Model formulation. AIChE J. 20:889–900. doi:10.1002/aic.690200509

Penrod, S.L., T.M. Olsen, and S.B. Grant. 1996. Deposition kinetics of two viruses in packed beds of quartz granular media. Langmuir 12:5576–5587. doi:10.1021/la950884d

Prieve, D.C., and M.M.J. Lin. 1980. Adsorption of Brownian hydrosols onto a rotating disc aided by a uniform applied force. J. Colloid Interface Sci. 76:32–47. doi:10.1016/0021-9797(80)90268-4

Rajagopalan, R., and C. Tien. 1976. Trajectory analysis of deep-bed filtration with the sphere-in-cell porous media model. AIChE J. 22:523–533. doi:10.1002/aic.690220316

Ryan, J.N., and M. Elimelech. 1996. Colloid mobilization and transport in groundwater. Colloids Surf. 107:1–56. doi:10.1016/0927-7757(95)03384-X

Saiers, J.E. 2002. Laboratory observations and mathematical modeling of colloid-facilitated contaminant transport in chemically heterogeneous systems. Water Resour. Res. 38(4):1032. doi:10.1029/2001WR000320

Saiers, J.E., and G.M. Hornberger. 1996. The role of colloidal kaolinite in the transport of cesium through laboratory sand columns. Water Resour. Res. 32:33–41. doi:10.1029/95WR03096

Saiers, J.E., and J.J. Lenhart. 2003. Ionic-strength effects on colloid transport and interfacial reactions in partially saturated porous media. Water Resour. Res. 39(9):1256. doi:10.1029/2002WR001887

Shen, C., Y. Huang, B. Li, and Y. Jin. 2010. Predicting attachment efficiency of colloid deposition under unfavorable attachment conditions. Water Resour. Res. 46:W11526. doi:10.1029/2010WR009218

Shen, C., B. Li, Y. Huang, and Y. Jin. 2007. Kinetics of coupled primary- and secondary-minimum deposition of colloids under unfavorable chemical conditions. Environ. Sci. Technol. 41:6976–6982. doi:10.1021/es070210c

Sirivithayapakorn, S., and A. Keller. 2003. Transport of colloids in unsaturated porous media: A pore-scale observation of processes during the dissolution of air–water interface. Water Resour. Res. 39:1346. doi:10.1029/2003WR002487

Snyder, L.J., and W.E. Stewart. 1966. Velocity and pressure profiles for Newtonian creeping flow in regular packed beds of spheres. AIChE J. 12:167–173. doi:10.1002/aic.690120130

Spielman, L.A., and J.A. Fitzpatrick. 1973. Theory of particle collection under London and gravity forces. J. Colloid Interface Sci. 42:607–623. doi:10.1016/0021-9797(73)90047-7

Thompson, S.S., M. Flury, M.V. Yates, and W.A. Jury. 1998. Role of the air–water–solid interface in bacteriophage sorption experiments. Appl. Environ. Microbiol. 64:304–309.

Tong, W.P., and W.P. Johnson. 2006. Excess colloid retention in porous media as a function of colloid size, fluid velocity, and grain angularity. Environ. Sci. Technol. 40:7725–7731. doi:10.1021/es061201r

Torkzaban, S., S.A. Bradford, and S.L. Walker. 2007. Resolving the coupled effects of hydrodynamics and DLVO forces on colloid attachment in porous media. Langmuir 23:9652–9660. doi:10.1021/la700995e

Torkzaban, S., S.L. Walker, and S.A. Bradford. 2009. Reply to comment by William P. Johnson et al. on "Transport and fate of bacteria in porous media: Coupled effects of chemical conditions and pore space geometry". Water Resour. Res. 45:W09604. doi:10.1029/2008WR007576

Unni, H.N., and C. Yang. 2005. Brownian dynamics simulation and experimental study of colloidal particle deposition in a microchannel flow. J. Colloid Interface Sci. 291:28–36. doi:10.1016/j.jcis.2005.04.104

Uthirakumar, P., E.K. Suh, C.H. Hong, and Y.S. Lee. 2005. Synthesis and characterization of polyesters containing fluorescein dye units. Polymer 46:4640–4646. doi:10.1016/j.polymer.2005.03.063

van Oss, C.J. 1994. Interfacial forces in aqueous media. Marcel Dekker, NY.

Verwey, E.J., and J.T.G. Overbeek. 1948. Theory of the stability of lyophobic colloids. Elsevier, Amsterdam.

Wan, J.M., and T.K. Tokunaga. 1997. Film straining of colloids in unsaturated porous media: Conceptual model and experimental testing. Environ. Sci. Technol. 31:2413–2420. doi:10.1021/es970017q

Wan, J.M., and J.L. Wilson. 1994. Visualization of the role of the gas–water interface on the fate and transport of colloids in porous media. Water Resour. Res. 30:11–23. doi:10.1029/93WR02403

Weisbrod, N., M.R. Niemet, and J.S. Selker. 2003. Light transmission technique for the evaluation of colloidal transport and dynamics in porous media. Environ. Sci. Technol. 37:3694–3700. doi:10.1021/es034010m

Wu, W. 2001. Baseline studies of The Clay Minerals Society source clays: Colloid and surface phenomena. Clays Clay Miner. 49:446–452. doi:10.1346/CCMN.2001.0490511

Wu, W., R.F. Giese, Jr., and C.J. van Oss. 1995. Evaluation of the Lifshitz–van der Waals/acid–base approach to determine surface tension components. Langmuir 11:379–382. doi:10.1021/la00001a064

Yiantsios, S.G., and A. Karabelas. 2003. Deposition of micron-sized particles on flat surfaces: Effects of hydrodynamic and physicochemical conditions on particle attachment efficiency. Chem. Eng. Sci. 58:3105–3113. doi:10.1016/S0009-2509(03)00169-6

Yu, D., R. Mei, L.-S. Luo, and W. Shyy. 2003. Viscous flow computations with the method of lattice Boltzmann equation. Prog. Aerosp. Sci. 39:329–367. doi:10.1016/S0376-0421(03)00003-4

Zevi, Y., A. Dathe, J.F. McCarthy, B.K. Richards, and T.S. Steenhuis. 2005. Distribution of colloid particles onto interfaces in partially saturated sand. Environ. Sci. Technol. 39:7055–7064. doi:10.1021/es048595b

Zhang, Z., and A. Prosperetti. 2003. A method for particle simulation. J. Appl. Mech. 70:64–74. doi:10.1115/1.1530636

Zhang, Z., and A. Prosperetti. 2005. A second-order method for three-dimensional particle simulation. J. Comput. Phys. 210:292–324. doi:10.1016/j.jcp.2005.04.009

Zhuang, J., Y. Jin, and M. Flury. 2003. Colloid-facilitated Cs transport through water-saturated Hanford sediment and Ottawa sand. Environ. Sci. Technol. 37:4905–4911. doi:10.1021/es0264504

Zhuang, J., J. Qi, and Y. Jin. 2005. Retention and transport of amphiphilic colloids under unsaturated flow conditions. Environ. Sci. Technol. 39:7853–7859. doi:10.1021/es050265j